A&A 564, A41 (2014)
DOI: 10.1051/0004-6361/201423491

Astronomy & Astrophysics

Stellar laboratories

II. New Zn IV and Zn V oscillator strengths and their validation in the hot white dwarfs G191−B2B and RE 0503−289⋆,⋆⋆,⋆⋆⋆

T. Rauch[1], K. Werner[1], P. Quinet[2,3], and J. W. Kruk[4]

[1] Institute for Astronomy and Astrophysics, Kepler Center for Astro and Particle Physics, Eberhard Karls University, Sand 1, 72076 Tübingen, Germany
e-mail: rauch@astro.uni-tuebingen.de
[2] Astrophysique et Spectroscopie, Université de Mons – UMONS, 7000 Mons, Belgium
[3] IPNAS, Université de Liège, Sart Tilman, 4000 Liège, Belgium
[4] NASA Goddard Space Flight Center, Greenbelt MD 20771, USA

Received 23 January 2014 / Accepted 3 March 2014

ABSTRACT

Context. For the spectral analysis of high-resolution and high-signal-to-noise (S/N) spectra of hot stars, state-of-the-art non-local thermodynamic equilibrium (NLTE) model atmospheres are mandatory. These are strongly dependent on the reliability of the atomic data that is used for their calculation. In a recent analysis of the ultraviolet (UV) spectrum of the DA-type white dwarf G191−B2B, 21 Zn IV lines were newly identified. Because of the lack of Zn IV data, transition probabilities of the isoelectronic Ge VI were adapted for a first, coarse determination of the photospheric Zn abundance.

Aims. Reliable Zn IV and Zn V oscillator strengths are used to improve the Zn abundance determination and to identify more Zn lines in the spectra of G191−B2B and the DO-type white dwarf RE 0503−289.

Methods. We performed new calculations of Zn IV and Zn V oscillator strengths to consider their radiative and collisional bound-bound transitions in detail in our NLTE stellar-atmosphere models for the analysis of the Zn IV − V spectrum exhibited in high-resolution and high-S/N UV observations of G191−B2B and RE 0503−289.

Results. In the UV spectrum of G191−B2B, we identify 31 Zn IV and 16 Zn V lines. Most of these are identified for the first time in any star. We can reproduce well almost all of them at $\log \mathrm{Zn} = -5.52 \pm 0.2$ (mass fraction, about 1.7 times solar). In particular, the Zn IV / Zn V ionization equilibrium, which is a very sensitive $T_{\rm eff}$ indicator, is well reproduced with the previously determined $T_{\rm eff} = 60\,000 \pm 2000$ K and $\log g = 7.60 \pm 0.05$. In the spectrum of RE 0503−289, we identified 128 Zn V lines for the first time and determined $\log \mathrm{Zn} = -3.57 \pm 0.2$ (155 times solar).

Conclusions. Reliable measurements and calculations of atomic data are a pre-requisite for stellar-atmosphere modeling. Observed Zn IV and Zn V line profiles in two white dwarf (G191−B2B and RE 0503−289) ultraviolet spectra were well reproduced with our newly calculated oscillator strengths. This allowed us to determine the photospheric Zn abundance of these two stars precisely.

Key words. atomic data – line: identification – stars: abundances – stars: individual: G191-B2B – virtual observatory tools – stars: individual: RE 0503-289

1. Introduction

In a recent spectral analysis of the hydrogen-rich DA-type white dwarf G191−B2B, Rauch et al. (2013) identified and reproduced stellar lines of C, N, O, Al, Si, O, P, S, Fe, Ni, Ge, and Sn. In addition, they identified 21 Zn IV lines. The determined Zn abundance (logarithmic mass fraction of −4.89, 7.5 × solar) was uncertain because the unknown Zn IV oscillator strengths were approximated by values of the isoelectronic Ge VI taken from Rauch et al. (2012).

In this paper, we introduce new oscillator strengths for Zn IV and Zn V (Sect. 2). Then, we describe briefly our observations (Sect. 3), our analysis strategy (Sect. 4), and revisit G191−B2B to perform a precise determination of its Zn abundance (Sect. 5). The white dwarf RE 0503−289 is hotter than G191−B2B and its trans-iron element abundances are strongly oversolar (Werner et al. 2012; Rauch et al. 2013) and, thus, it appears promising to identify Zn lines. In Sect. 6, we describe our search for these and the determination of its Zn abundance. We summarize our results and conclude in Sect. 7.

2. Transition probabilities in Zn IV and Zn V

Radiative decay rates (oscillator strengths and transition probabilities) have been computed using the pseudo-relativistic Hartree-Fock (HFR) method as described by Cowan (1981).

⋆ Based on observations with the NASA/ESA *Hubble* Space Telescope, obtained at the Space Telescope Science Institute, which is operated by the Association of Universities for Research in Astronomy, Inc., under NASA contract NAS5-26666.

⋆⋆ Based on observations made with the NASA-CNES-CSA Far Ultraviolet Spectroscopic Explorer.

⋆⋆⋆ Tables 1 and 2 are only available at the CDS via anonymous ftp to cdsarc.u-strasbg.fr (130.79.128.5) or via http://cdsarc.u-strasbg.fr/viz-bin/qcat?J/A+A/564/A41

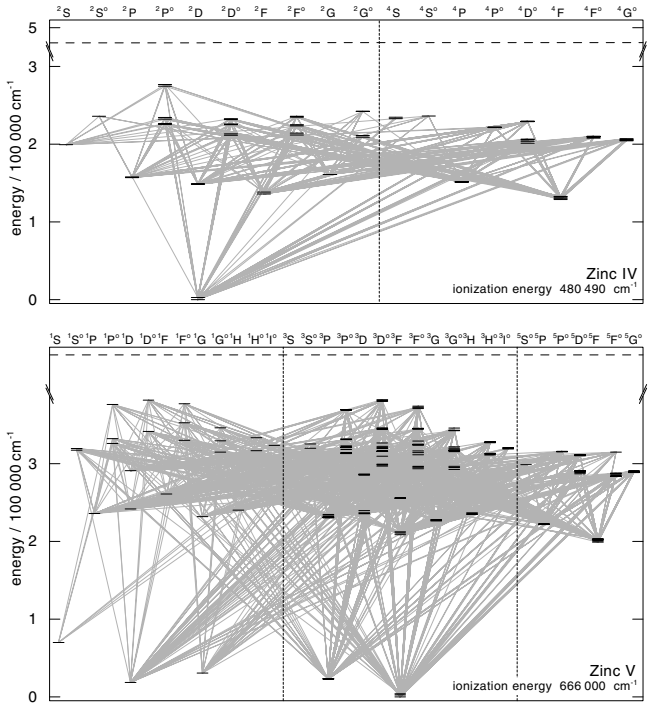

Fig. 1. Grotrian diagrams of our Zn IV (*top*) and Zn V (*bottom*) model ions. Horizontal bars indicate levels, gray lines represent radiative transitions with known f values, respectively. The dashed lines show the ionization energies.

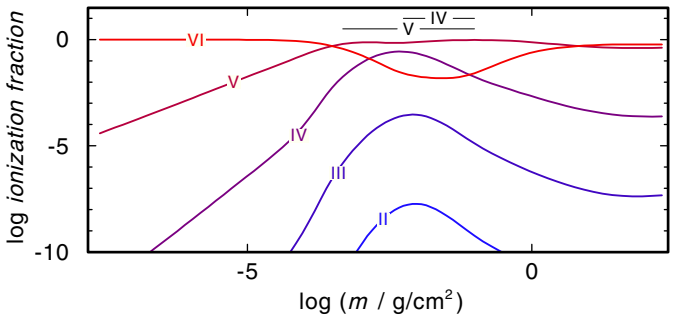

Fig. 2. Ionization fractions of Zn II – VI in our G191−B2B model atmosphere. m is the column mass, measured from the outer boundary of our model atmosphere. The formation depths (i.e., $\tau = 1$) of the Zn IV – V line cores are marked.

Table 3. Statistics of our N, O, and Zn model atoms for G191−B2B.

Ion	NLTE levels	LTE levels	Lines
N II	1	246	0
III	9	57	10
IV	9	85	10
V	10	52	20
VI	1	0	0
O II	1	46	0
III	9	63	6
IV	9	85	11
V	9	117	12
VI	10	75	19
VII	1	0	0
Zn II	6	0	8
III	13	0	17
IV	63	13	399
V	157	0	1878
VI	1	0	0

For Zn IV, configuration interaction has been considered among the configurations $3d^9$, $3d^84s$, $3d^85s$, $3d^84d$, $3d^85d$, $3d^74s^2$, $3d^74p^2$, $3d^74d^2$, $3d^74f^2$, $3d^74s5s$, $3d^74s4d$, and $3d^74s5d$ for the even parity and $3d^84p$, $3d^85p$, $3d^84f$, $3d^85f$, $3d^74s4p$, $3d^74s5p$, $3d^74s4f$, $3d^74s5f$, and $3d^74p4d$ for the odd parity. Using experimental energy levels published by Sugar & Musgrove (1995), the average energies ($E_{\rm av}$), the Slater integrals ($F^{\rm k}$, $G^{\rm k}$), the spin-orbit parameters ($\zeta_{\rm nl}$), and the effective interaction parameters (α, β) corresponding to $3d^9$, $3d^84s$, $3d^84p$ configurations were optimized using a well-established least-squares fitting process minimizing the differences between calculated and experimental energy levels within both configurations. In the case of Zn V, the configurations included in the HFR model were $3d^8$, $3d^74s$, $3d^75s$, $3d^74d$, $3d^75d$, $3d^64s^2$, $3d^64p^2$, $3d^64d^2$, $3d^64s5s$, $3d^64s4d$, $3d^64s5d$ for the even parity and $3d^74p$, $3d^75p$, $3d^74f$, $3d^75f$, $3d^64s4p$, $3d^64s5p$, $3d^64s4f$ and $3d^64p4d$ for the odd parity. For this ion, the semi-empirical fitting process was performed to optimize the radial integrals corresponding to $3d^8$, $3d^74s$, and $3d^74p$ configurations using the experimental energy levels compiled by Sugar & Musgrove (1995). The HFR oscillator strengths ($\log gf$) and transition probabilities (gA, in s^{-1}) for Zn IV and Zn V spectral lines are reported in Tables 1 and 2, respectively, alongside with the numerical values (in cm^{-1}) of lower and upper energy levels and the corresponding wavelengths (in Å). In the last column of each table, we also give the cancellation factor CF as defined by Cowan (1981). We note that very small values of this factor (typically <0.05) indicate strong cancellation effects in the calculation of line strengths. In these cases, the corresponding gf and gA values could be very inaccurate and so need to be considered with some care. However, very few transitions appearing in Tables 1 and 2 are affected by these effects. Figure 1 shows Grotrian diagrams of Zn IV and Zn V including all levels and transitions from Tables 1 and 2.

3. Observations

In this analysis, we use the FUSE[1] spectrum of RE 0503−289 and the FUSE and HST/STIS[2] spectra G191−B2B that are described in detail by Werner et al. (2012) and Rauch et al. (2013), respectively.

Both FUSE spectra are co-added from all available observations of RE 0503−289 and G191−B2B. They cover the wavelength range 910 Å $< \lambda <$ 1188 Å. Their resolving power is $R = \lambda/\Delta\lambda \approx 20\,000$. The HST/STIS spectrum of G191−B2B is co-added from 105 observation with the highest resolution (grating E140H, $R \approx 118\,000$, 1145 Å $< \lambda <$ 1700 Å) available via MAST.

4. Model atmospheres and atomic data

To determine the Zn abundance of G191−B2B, it would be straightforward to use the final model of Rauch et al. (2013) as well as their model atoms with the only exception that the Zn IV and Zn V model ions were replaced by the extended versions that consider the newly calculated transition probabilities

[1] Far Ultraviolet Spectroscopic Explorer.

[2] *Hubble* Space Telescope/Space Telescope Imaging Spectrograph, for our high-resolution spectrum of G191−B2B, see http://www.stsci.edu/hst/observatory/crds/calspec.html

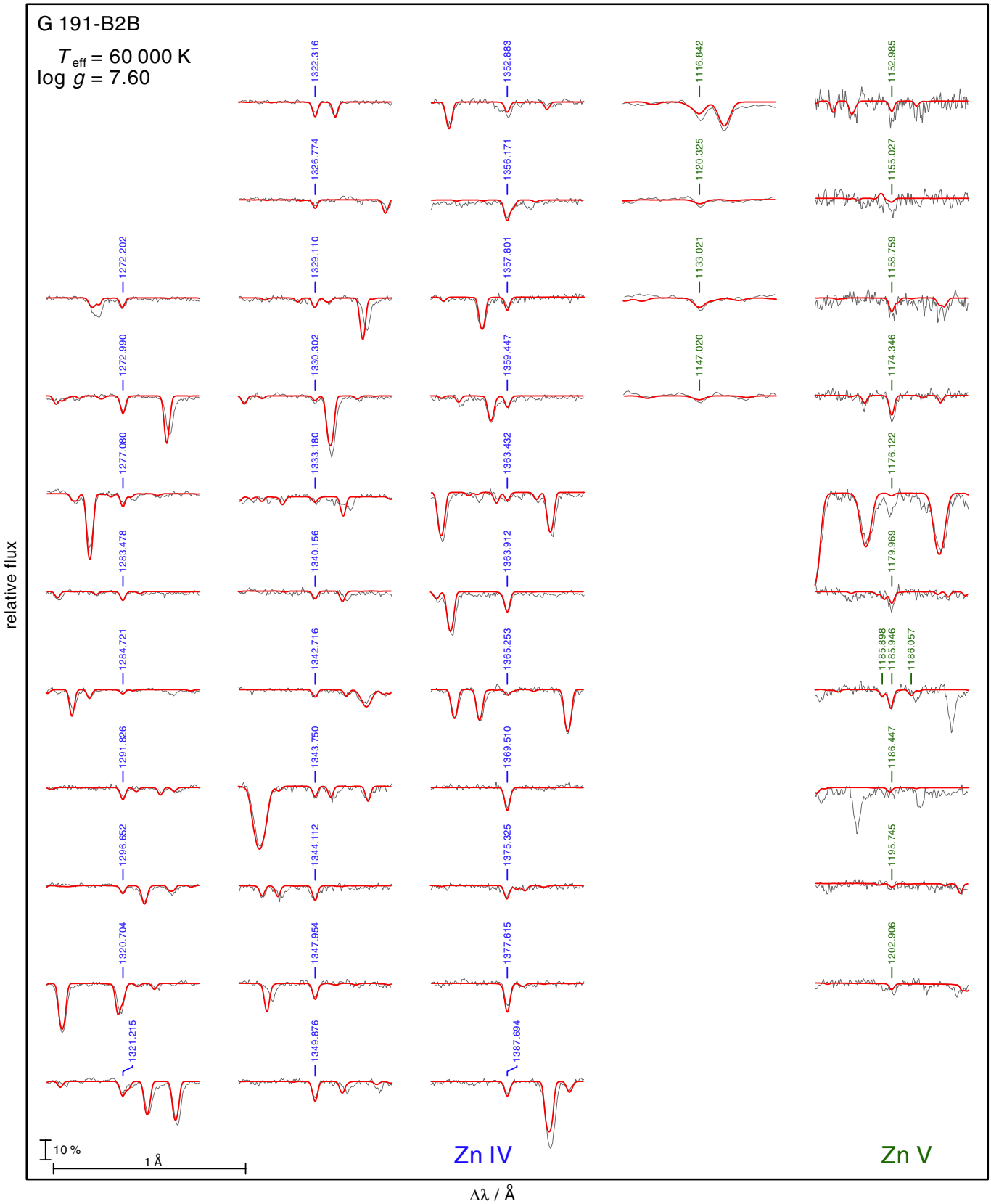

Fig. 3. Zn IV lines (*left panel*, marked with their wavelengths in Å, blue in the online version) and Zn V lines (*right panel*, marked in green) in the FUSE (for lines at $\lambda < 1150$ Å) and HST/STIS ($\lambda > 1150$ Å) observations of G191−B2B compared with our theoretical line profiles. For the identification of other lines, see Rauch et al. (2013). The vertical bar shows 10% of the continuum flux.

Table 4. Identified Zn lines in the UV spectrum of G191−B2B.

Ion		Wavelength/Å		Comments
		Theoretical	Observed	
Zn	IV	1272. 202		
		1272. 990	1272.975	prev. unid.
		1277. 080	1277.130	$\Delta\lambda > 0.02$ Å
		1283. 478	1283.525	$\Delta\lambda > 0.02$ Å, prev. unid.
		1284. 721	1284.740	
		1291. 826	1291.810	
		1296. 652	1296.620	
		1320. 704	1320.725	
		1321. 215		
		1322. 316	1322.320	
		1326. 774	1326.735	$\Delta\lambda > 0.02$ Å
		1329. 110		
		1330. 302	1330.325	
		1333. 180		
		1340. 156	1340.190	$\Delta\lambda > 0.02$ Å
		1342. 716	1342.755	$\Delta\lambda > 0.02$ Å
		1343. 750	1343.815	$\Delta\lambda > 0.02$ Å
		1344. 122	1344.090	$\Delta\lambda > 0.02$ Å
		1347. 954	1347.970	
		1349. 876	1349.895	
		1352. 883	1352.905	$\Delta\lambda > 0.02$ Å
		1356. 171	1356.090	$\Delta\lambda > 0.02$ Å, blend with Zn IV λ 1356.195 Å
		.	.	
		1357. 801	1357.810	
		1359. 477	1359.490	
		1363. 432	1363.420	
		1363. 912	1363.940	$\Delta\lambda > 0.02$ Å
		1365. 253	1365.260	
		1369. 510	1369.515	
		1375. 325		
		1377. 615	1377.635	
		1387. 694	1387.720	
Zn	V	1116. 842	1116.860	
		1120. 325	1120.330	
		1133. 031	1133.060	$\Delta\lambda > 0.02$ Å, prev. unid.
		1147. 020	1147.040	
		1152. 985	1152.980	
		1155. 027	1155.045	
		1158. 759	1158.750	prev. unid.
		1174. 346	1174.325	prev. unid.
		1176. 122		weak, prev. unid.
		1179. 969	1180.005	$\Delta\lambda > 0.02$ Å
		1185. 898	1185.905	
		1185. 948	1185.955	
		1186. 057		
		1186. 447		weak, prev. unid.
		1195. 745		weak
		1202. 906		

Notes. Observed wavelengths are given only in case that they deviate from the theoretical wavelengths (cf. Tables 1 and 2). "prev. unid." denotes lines that were previously listed as unidentified by Rauch et al. (2013).

(Sect. 2). Unfortunately, the employed Tübingen non-local thermodynamic equilibrium (NLTE) model-atmosphere package (Werner et al. 2003; Rauch & Deetjen 2003, TMAP[3]), which

[3] http://astro.uni-tuebingen.de/~TMAP

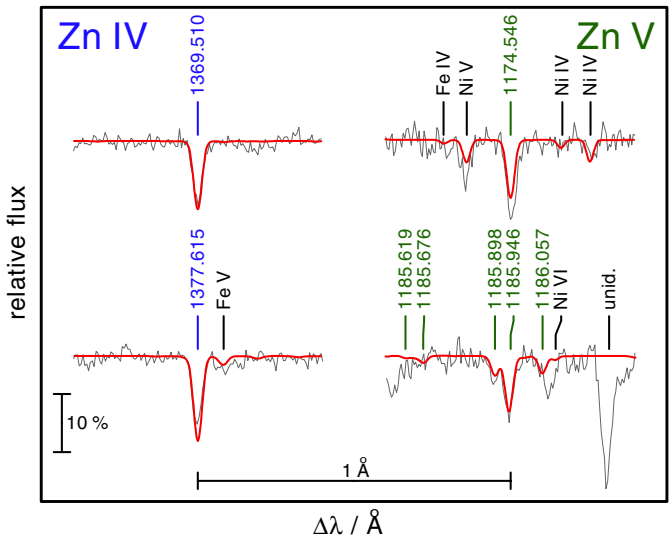

Fig. 4. Theoretical line profiles of the strongest Zn IV lines (*left*) and Zn V lines (*right*) (marked with their wavelengths from Tables 1 and 2) calculated from our model of G191−B2B with a Zn abundance of 3.0×10^{-6} (mass fraction) located in the STIS wavelength range compared with the observation. The lines are shifted to the observation, see Table 4.

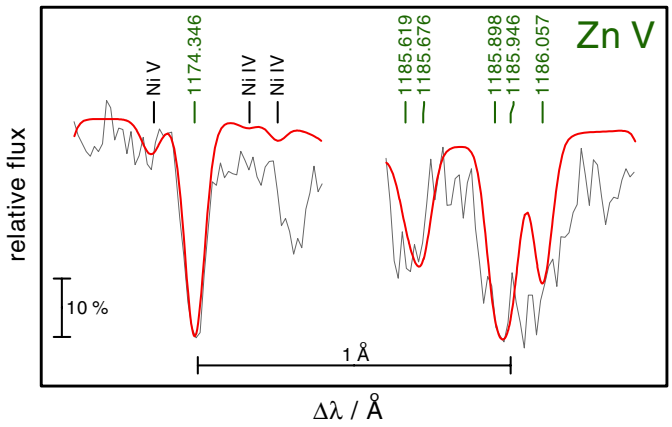

Fig. 5. Theoretical line profiles of the strongest Zn V lines calculated from our model of RE 0503−289 with a Zn abundance of 2.7×10^{-4} (mass fraction) located in the FUSE wavelength range compared with the observation. The lines are shifted to the observation, see Table 5.

is used to calculate plane-parallel, chemically homogeneous, metal-line blanketed NLTE model atmospheres, overcharged our FORTRAN compilers. The program would not compile if the array sizes were increased further according to the much higher number of atomic levels treated in NLTE and the respective higher number of radiative and collisional transitions.

Thus, we decided to reduce the number of N and O levels treated in NLTE (Table 3) to create a TMAP executable. Test calculations have shown that the deviations in temperature and density structure between the final model of Rauch et al. (2013) and a model with reduced N and O model atoms are negligible. Then, the Zn occupation numbers are determined in a line-formation calculation, i.e., at fixed temperature and density structure. Since Zn opacities were already considered in our start model, the atmospheric structure and the background opacities are well modeled.

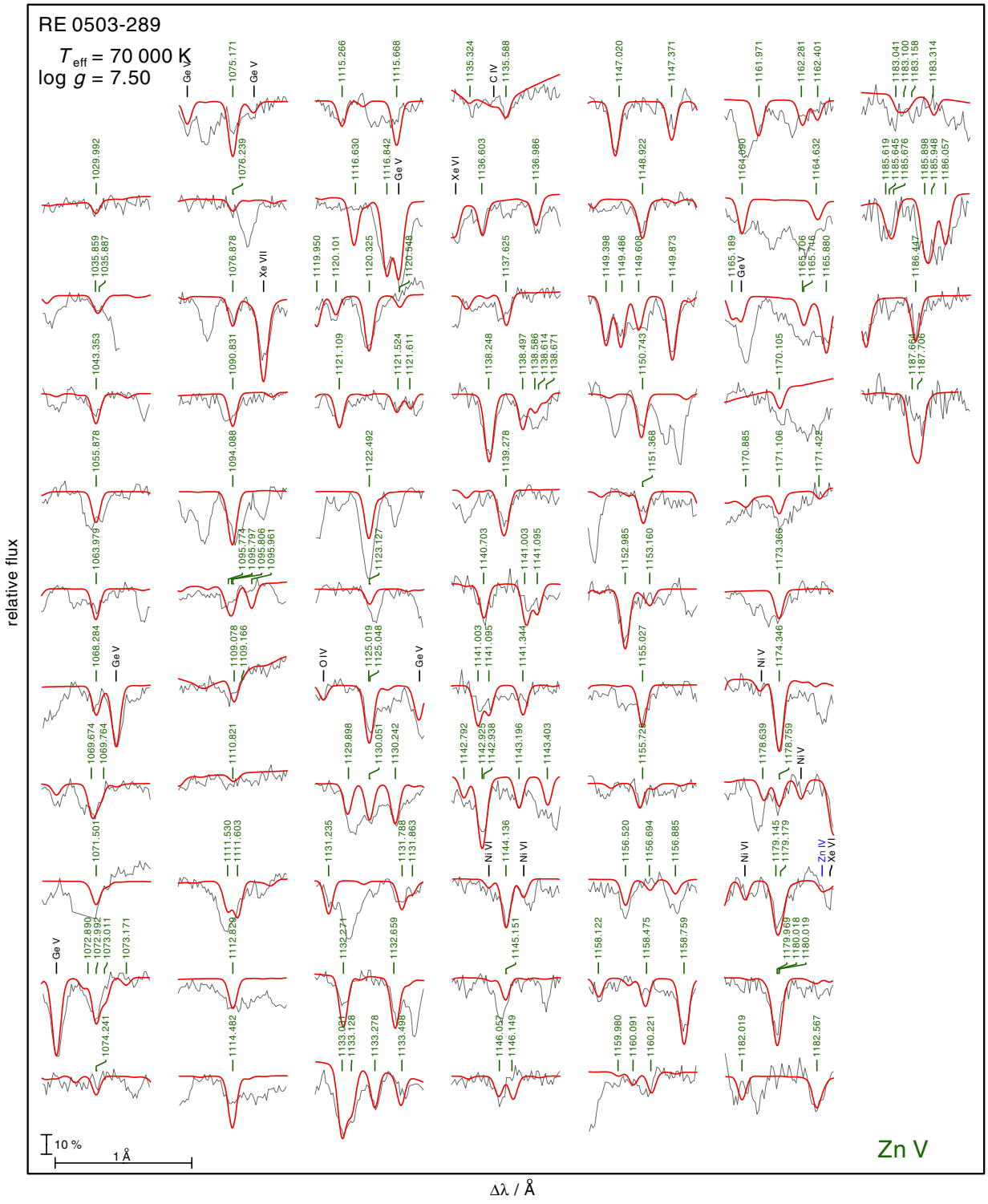

Fig. 6. Zn V lines in the FUSE observation of RE 0503−289 compared with our theoretical line profiles.

All model atoms (including Zn) are provided via the Tübingen Model-Atom Database (TMAD[4], Rauch & Deetjen 2003), that has been set up within a project of the German Astrophysical Virtual Observatory (GAVO[5]). All SEDs that were calculated for this analysis are available via the registered Theoretical Stellar Spectra Access (TheoSSA[6]) VO service.

[4] http://astro.uni-tuebingen.de/~TMAD
[5] http://www.g-vo.org
[6] http://dc.g-vo.org/theossa

5. The photospheric Zn abundance in G191−B2B

Zn IV and Zn V are the dominant ionization stages of Zn in the atmosphere of G191−B2B (Fig. 2). Therefore, we closely inspected the available spectra for lines of these ions.

In the FUSE and HST/STIS observations of G191−B2B (cf. Rauch et al. 2013) we identified 31 Zn IV (10 new identifications) and 16 Zn V (all new) lines. The observed wavelength positions (a radial velocity of $v_{\rm rad}$ = 22.1 km s^{-1} was applied according to Holberg et al. 1994; Rauch et al. 2013) deviate partly from

Table 5. Like Table 4, for RE 0503−289.

Ion	Wavelength/Å		Comments
	Theoretical	Observed	
Zn V	1029. 992		
	1035. 859		
	1035. 887		
	1043. 353		
	1055. 878		
	1063. 979		
	1068. 284		
	1069. 674		blend with O V, Ga V, Ge V
	1069. 764		
	1071. 501		
	1072. 992	1072.950	$\Delta\lambda > 0.02$ Å
	1074. 241	1074.265	$\Delta\lambda > 0.02$ Å
	1075. 171	1075.050	$\Delta\lambda > 0.02$ Å
	1076. 239		
	1076. 878	1076.895	
	1090. 831	1090.800	$\Delta\lambda > 0.02$ Å
	1094. 088	1094.110	blend with N IV
	1095. 774		blend with Ge V
	1095. 797		
	1095. 961	1095.945	
	1109. 078	1109.110	$\Delta\lambda > 0.02$ Å blend with C IV
	1109. 166		blend with C IV
	1110. 821	1110.810	weak
	1111. 530		blend with C III, O IV
	1111. 603		
	1112. 829		
	1114. 482		
	1115. 266	1115.295	$\Delta\lambda > 0.02$ Å
	1115. 668	1115.695	$\Delta\lambda > 0.02$ Å
	1116. 630		too strong in model
	1116. 842	1116.860	
	1119. 950	1119.940	
	1120. 101	1120.080	$\Delta\lambda > 0.02$ Å
	1120. 325		
	1121. 109	1121.095	
	1121. 524		weak
	1122. 502		blend with Si IV
	1123. 127		blend with Ga V
	1125. 019	1125.050	$\Delta\lambda > 0.02$ Å
	1125. 048	1125.060	
	1129. 898		blend with Ga V
	1130. 051		
	1130. 242		
	1131. 242	1131.250	prev. unid.
	1131. 788		
	1131. 863		
	1132. 271	1132.290	
	1132. 659		blend with N IV
	1133. 031	1133.060	$\Delta\lambda > 0.02$ Å
	1133. 128		
	1133. 278	1133.300	$\Delta\lambda > 0.02$ Å
	1133. 498		
	1135. 324		
	1135. 588		
	1136. 603		
	1136. 986	1137.000	
	1137. 625		

Table 5. continued.

Ion	Wavelength/Å		Comments
	Theoretical	Observed	
	1138. 248		
	1138. 497		
	1139. 278	1139.220	$\Delta\lambda > 0.02$ Å blend with Ge V
	1140. 703		
	1141. 003	1141.015	
	1141. 095		
	1141. 344		
	1142. 792		
	1142. 925		
	1142. 938		prev. unid.
	1143. 196		
	1143. 403		
	1144. 136	1144.160	$\Delta\lambda > 0.02$ Å
	1145. 151		
	1146. 057		
	1146. 149		too strong in model
	1147. 020	1147.040	
	1147. 371	1147.425	$\Delta\lambda > 0.02$ Å
	1148. 922	1148.915	
	1149. 398	1149.370	$\Delta\lambda > 0.02$ Å
	1149. 486		
	1149. 608		
	1149. 873	1149.855	
	1150. 743		
	1151. 368		
	1152. 985	1152.980	
	1153. 160		
	1155. 027	1155.045	
	1155. 725	1158.750	
	1156. 520		
	1156. 885		
	1158. 122		
	1158. 475		
	1158. 759	1158.750	
	1160. 091		weak
	1160. 221		
	1161. 971		
	1162. 281		
	1162. 401		
	1164. 090		blend of Zn V $\lambda\lambda$ 1165.082, 1164.101 Å
	1164. 632		blend with O IV
	1165. 189		
	1165. 706		blend with C III
	1165. 716		blend with C III
	1165. 880		blend with Xe VI
	1170. 105		
	1171. 106	1171.130	
	1173. 366		
	1174. 346	1174.325	
	1174. 945		blend with C III
	1176. 122		blend with C III
	1178. 759		
	1179. 145		
	1179. 179		
	1179. 969	1180.005	$\Delta\lambda > 0.02$ Å

Table 5. continued.

Ion	Wavelength/Å		Comments
	Theoretical	Observed	
	1180. 018		blend of Zn V $\lambda\lambda$ 1180.018, 1180.025 Å
	1182. 019		
	1182. 567		
	1183. 041		
	1183. 100		
	1183. 158		
	1183. 314		
	1185. 619		
	1185. 645		
	1185. 676		
	1185. 898	1185.905	
	1185. 948	1185.955	blend of Zn V $\lambda\lambda$ 1185.948, 1185.961 Å
	1186. 057		
	1186. 447	1186.420	$\Delta\lambda > 0.02$ Å
	1187. 664		too strong in model
	1187. 706		too strong in model

those given in Tables 1 and 2 by some hundredths of an Å. The good agreement of the strongest, unshifted lines in our model[7] (Fig. 3) with the observations permits to shift the lines to observed absorption features in their closest vicinity. The reason for this uncertainty is most likely the limited accuracy of the Zn IV and Zn V energy levels from which the wavelengths of the line transitions were calculated. The identified lines are summarized in Table 4.

Our calculations have shown that the Zn IV / Zn V ionization equilibrium at $T_{\rm eff} = 60\,000$ K and $\log g = 7.6$ (cf. Rauch et al. 2013) is well reproduced (Figs. 3, 4). On the other hand, the Zn abundance given by Rauch et al. (2013, $1.3 \times 10^{-5} \pm 0.5$ dex by mass) is too high. We reduced it to $3.0 \times 10^{-6} \pm 0.2$ dex (about 1.7 times solar, following Asplund et al. 2009) to reproduce the observed Zn lines best. This agrees with the previous value within the error limits. Even a solar Zn abundance, however, is possible within the error limits.

6. The photospheric Zn abundance in RE 0503−289

Our inspection of all UV spectra that were already used by Werner et al. (2012) has shown that only RE 0503−289 exhibits prominent Zn lines (Fig. 5). We find that in its FUSE spectrum ($v_{\rm rad} = 26.3\,{\rm km\,s^{-1}}$), a rich Zn V spectrum of 128 lines (Fig. 6, Table 5) is present. The synthetic spectrum of our final model shows more, weak lines that do not have an unambiguous line identification due to the signal-to-noise ratio (S/N) of the observation. The model's prediction of their relative line strengths facilitates to distinguish between noise and "real" lines in the observation and, hence, to identify even such weak lines. In general, all lines with oscillator strengths $gf \gtrsim 0.01$ can be detected.

Dreizler & Werner (1996) determined $T_{\rm eff} = 70\,000 \pm 4000$ K and $\log g = 7.50 \pm 0.25$ for RE 0503−289. This was recently verified by well-matched ionization equilibria of Kr and Xe (Werner et al. 2012, Kr VI / Kr VII, Xe VI / Xe VII) and Ge (Rauch et al. 2012, Ge V / Ge VI). We adopt these values and start our calculation based on the final model of Werner et al. (2012) that considers opacities of He, C, N, O, Ge, Kr, Xe, and of the iron-group elements (Ca - Ni). We follow the same strategy described in Sect. 4, but this time, we reduced the size of the Ge model atom in the line-formation calculations.

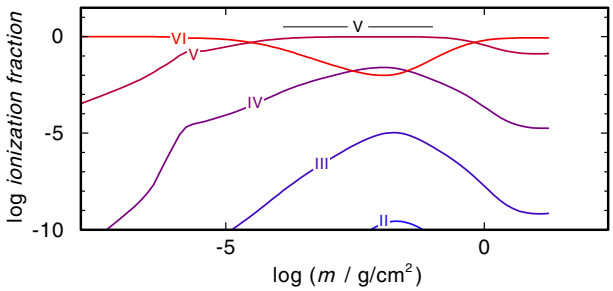

Fig. 7. Like Fig. 2, for our RE 0503−289 model atmosphere.

The higher $T_{\rm eff}$ compared to that of G191−B2B shifts the Zn ionization equilibrium strongly towards higher ionization (Fig. 7). Zn V remains dominant while Zn IV is less occupied by a factor of about 100 at all depths. The ionization fraction of Zn VI is also much below that of Zn V and we only expect weak lines. The strongest Zn VI lines[8] are located in the soft X-ray to EUV[9] wavelength range where we do not have high-quality observations to evaluate.

We determine a Zn abundance of $2.7 \times 10^{-4} \pm 0.2$ dex (about $155\times$ solar) to reproduce the observed Zn V line profiles best (Fig. 5).

7. Results and conclusions

The identified Zn IV and Zn V lines in the high-resolution UV spectra of G191−B2B and RE 0503−289 are well reproduced with our newly calculated oscillator strengths by our NLTE model-atmosphere calculations.

We determined photospheric abundances of $\log {\rm Zn} = -5.52 \pm 0.2$ (mass fraction, $1.9–4.8 \times 10^{-6}$, 1.1–2.8 times the solar abundance) and $\log {\rm Zn} = -3.57 \pm 0.2$ ($1.7–4.3 \times 10^{-4}$, 98–248 times solar) for the DA-type white dwarf G191−B2B and the DO-type white dwarf RE 0503−289, respectively. The highly supersolar Zn abundance is in line with the high abundances of trans-iron elements Ge ($650\times$ solar, Rauch et al. 2012), Kr ($450\times$ solar), Xe ($3800\times$ solar, Werner et al. 2012) in RE 0503−289.

The identification of new lines due to trans-iron elements, e.g., Ga, Ge, As, Se, Kr, Mo, Sn, Te, I, and Xe (Werner et al. 2012) and Zn (Rauch et al. 2013, and in this paper) in G191−B2B and RE 0503−289 promises to help enhance the understanding of extremely metal-rich white dwarf photospheres and their relation to AGB and post-AGB stellar evolution. Their reproduction, i.e., the precise abundance determination, e.g., of Kr and Xe (Werner et al. 2012), Ge and Sn (Rauch et al. 2012), and Zn (this paper) is strongly dependent on the available atomic data. This remains a challenge for atomic and theoretical physicists.

Acknowledgements. T.R. is supported by the German Aerospace Center (DLR, grant 05 OR 0806). Financial support from the Belgian FRS-FNRS is also acknowledged. PQ is research director of this organization. This research has made use of the SIMBAD database, operated at CDS, Strasbourg, France. Some of the

[7] All synthetic spectra shown in this paper are convolved with Gaussians to match the spectral resolution (FUSE: $FWHM = 0.06$ Å, STIS: $FWHM = 0.01$ Å).

[8] http://www.pa.uky.edu/~peter/atomic

[9] Extreme ultraviolet.

data presented in this paper were obtained from the Mikulski Archive for Space Telescopes (MAST). STScI is operated by the Association of Universities for Research in Astronomy, Inc., under NASA contract NAS5-26555. Support for MAST for non-HST data is provided by the NASA Office of Space Science via grant NNX09AF08G and by other grants and contracts.

References

Asplund, M., Grevesse, N., Sauval, A. J., & Scott, P. 2009, ARA&A, 47, 481
Cowan, R. D. 1981, The theory of atomic structure and spectra (Berkeley, CA: University of California Press)
Dreizler, S., & Werner, K. 1996, A&A, 314, 217
Holberg, J. B., Hubeny, I., Barstow, M. A., et al. 1994, ApJ, 425, L105
Rauch, T., & Deetjen, J. L. 2003, in Stellar Atmosphere Modeling, eds. I. Hubeny, D. Mihalas, & K. Werner, ASP Conf. Ser., 288, 103
Rauch, T., Werner, K., Biémont, É., Quinet, P., & Kruk, J. W. 2012, A&A, 546, A55
Rauch, T., Werner, K., Bohlin, R., & Kruk, J. W. 2013, A&A, 560, A106
Sugar, J., & Musgrove, A. 1995, J. Phys. Chem. Ref. Data, 24, 1803
Werner, K., Deetjen, J. L., Dreizler, S., et al. 2003, in Stellar Atmosphere Modeling, eds. I. Hubeny, D. Mihalas, & K. Werner, ASP Conf. Ser., 288, 31
Werner, K., Rauch, T., Ringat, E., & Kruk, J. W. 2012, ApJ, 753, L7